

Fabrication of Highly Uniform Gold Nanoparticles-Titanium Dioxide Nanotube Arrays for H₂O₂ Sensing

Chokchai PUTTHARUGSA[†] and Areeya AEIMBHU

Physics Department, Faculty of Science, Srinakharinwirot University, 114 Sukhvit 23 Wattana, 10110 Bangkok, Thailand

This research was to prepare the titanium dioxide nanotube arrays (TiNT arrays) and deposit the Au nanoparticles on its surface using the pulse electrodeposition technique. The Au nanoparticles-TiNT arrays (AuNP-TiNT arrays) were characterized by field emission scanning electron microscopy (FESEM), X-ray diffraction, and cyclic voltammetry. The results showed that the Au nanoparticles were uniformly dispersed on the TiNT array surface. The size and loading of Au nanoparticles can be controlled by deposition time, deposition potential, and concentration of HAuCl₄. The AuNP-TiNT arrays were then used as a working electrode for hydrogen peroxide (H₂O₂) detection. Compared with the pure TiNT array electrode, the AuNP-TiNT array electrode had higher sensitivity for the detection of H₂O₂ and thus provided a simple, promising, and cost-effective sensing platform for the development of enzyme-based biosensors.

Keywords Titanium dioxide nanotube arrays, Au nanoparticles, pulse electrodeposition, H₂O₂ sensing

(Received August 22, 2017; Accepted October 13, 2017; Published March 10, 2018)

Introduction

Titanium dioxide nanotube arrays (TiNT arrays) are widely used in many applications because of their geometry and functionality. The benefits of TiNT arrays include (1) a large surface area, (2) a high pore volume, (3) excellent adhesion, and (4) excellent electron pathway.¹ With a facile synthesis process, the high order of TiNT arrays can be simply prepared by anodization of titanium (titanium foil or sheet). Thus, it can be seen that TiNT arrays have been widely used in many applications, such as gas sensors, solar cells, photocatalysis, tissue engineering, and biosensors.²⁻⁶ In biosensor development, hydrogen peroxide (H₂O₂), the product of enzymatic reaction, is recognized as a major factor. Generally, enzyme biosensors (such as glucose oxidase, horseradish peroxidase, myoglobin, and hemoglobin) are based on the detection of H₂O₂ and electrons directly transferring between electrodes and proteins.⁷⁻¹⁰ Enzymes are usually modified on the TiNT array electrode for detecting a low concentration of H₂O₂ or a high sensitivity to H₂O₂. However, the TiNT array-based electrode has poor electrical conductivity and a higher detection potential for H₂O₂ sensing. Thus, the improvement of electrical properties for the TiNT array electrode is important in the development of H₂O₂ sensing. To improve its property, for example, Xie and Zhao used a conducting polymer (polypyrrole) to coat the TiNT array surface for developing a glucose biosensor.¹¹ Alternatively, one effective method is to load a noble metal, especially gold nanoparticles, onto the TiNT array surface. This is because Au nanoparticles have a good catalytic activity on the supporting material, depending on the particle size, dispersion, and composition.¹²

Previous reports have studied the preparation of metal nanoparticles (Au, Ag, or Cu) on the TiNT surface, including sputtering,¹³ photo-reduction,¹⁴⁻¹⁶ deposition-precipitation,^{17,18} and electrodeposition.^{19,20} Although these methods can successfully prepare the nanoparticles on the TiNT surface, the nanoparticles will easily aggregate and grow large on the surface of the TiNT array. To enhance catalytic activity, the metal nanoparticle should be sufficiently small and homogeneously disperse on the TiNT array surface. Thus, an effective method needs to be chosen to modify the nanoparticle on the surface.

Recently, Lai and colleagues successfully prepared the Ag nanoparticles on the TiNT array surface by using the pulse current deposition technique.²¹ Moreover, this technique was also used to load Au and Ni/Cu nanoparticles on the TiNT array surface for biosensor and photoelectrocatalytic activity, respectively.^{22,23} The obtained nanoparticles homogeneously dispersed on the TiNT surface with a small size. In this technique, the potential/current is applied to the TiNT electrode. The potential/current, controlled by a potentiostat, is rapidly alternated between two different values. This is called a potential pulse or a current pulse. The pulse consists of two periods including an on-time (t_{on}) period and an off-time (t_{off}) period. In the t_{on} period, the potential/current is applied at one value while in the t_{off} period, the potential/current is applied at another value to the electrode. The advantages of this technique are (1) easy control of the size and dispersion of the nanoparticle on the surface by changing the applied potential/current, $t_{\text{on}}/t_{\text{off}}$ period, and deposition time (pulse cycles) and (2) replenishment of the metal ion into the diffusion layer during the t_{off} period due to the limiting current density.²⁴ Thus, pulse electrodeposition is a suitable technique to fabricate uniform Au nanoparticles on the TiNT array surface.

The objective of this research was to prepare the TiNT array layer and then load Au nanoparticles to the TiNT array surface

[†] To whom correspondence should be addressed.
E-mail: chokchai@g.swu.ac.th

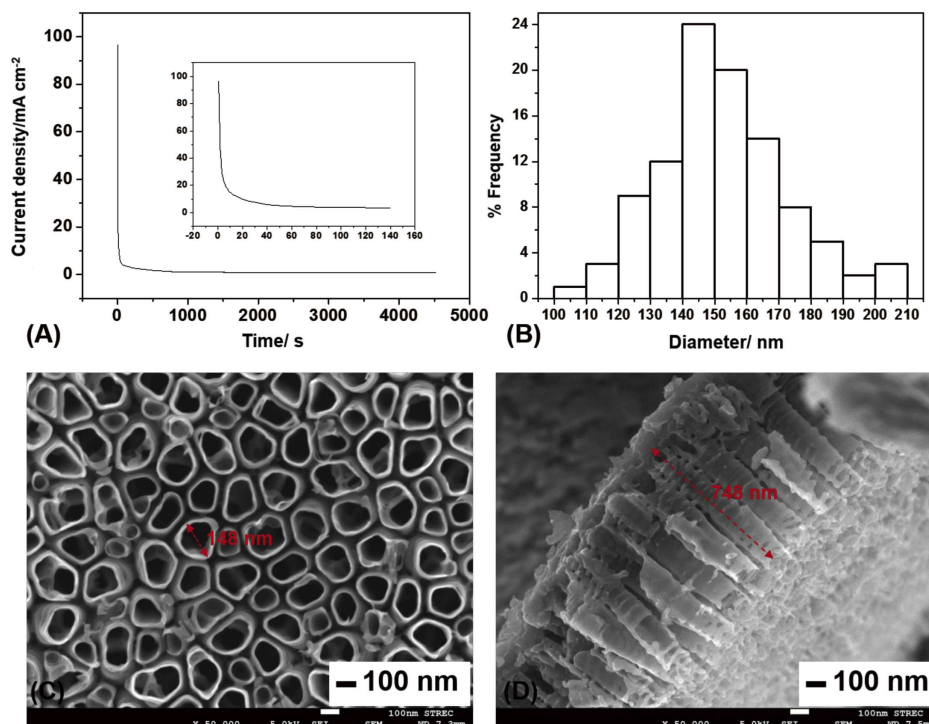


Fig. 1 (A) The relationship between current density and time in the process of anodization. (B) The distribution of TiNT array diameter. SEM image of TiNT array in (C) top view and (D) cross-section.

through pulse electrodeposition. The size and amount of Au nanoparticles were controlled by various parameters such as electrolyte concentration, potential pulse, and deposition time. Furthermore, the AuNP-TiNT arrays were then used as a working electrode for H₂O₂ sensing.

Experimental

Materials

Titanium foil (grade 2) was purchased from Miracle Metal (Thailand). Ammonium fluoride (NH₄F), ethylene glycol, and hydrogen peroxide (H₂O₂) were purchased from Italmar (Thailand). Hydrogen tetrachloroaurate (HAuCl₄) was purchased from Aldrich (Singapore). Other chemicals were analytical grade and were used without purification. Deionized water was used throughout the experiment.

Preparation of TiNT arrays

A titanium foil was cut to 1.0 × 1.0 cm². Prior to anodization, the foil was degreased in an ultrasonic bath in anhydrous ethanol and deionized (DI) water for 5 min, successively, and then rinsed with DI water and dried with nitrogen gas. The cleaned titanium foil was then placed on the Teflon chamber with a rubber O-ring (8.0 mm in diameter) to prevent electrolyte leakage. The other side of the titanium foil was used as an electrical contact to a silver wire. Anodization was carried out for 1.5 h in ethylene glycol/water (50:50) electrolyte containing 1.0% (w/v) NH₄F at 25 V against a platinum wire coil serving as the counter electrode. After anodization, the TiNT array layers were cleaned in the ultrasonic bath in DI water and dried with nitrogen gas. The as-anodized amorphous TiNT was subsequently annealed at 500°C in air for 90 min with a ramping rate of 10°C/min and then cooled at 5°C/min to induce the formation of crystalline anatase.

Pulse electrodeposition

Pulse electrodeposition of Au nanoparticles on TiNT arrays was carried out using the Autolab potentiostat (μAutolab FRAIII, Eco Chemie, The Netherlands) for controlling the deposition potential and deposition time. The experiment was performed at room temperature (25 ± 1°C). A three-electrode setup was applied using the TiNT arrays, a platinum coil, and an Ag/AgCl electrode as the working electrode, counter electrode, and reference electrode, respectively. The TiNT array working electrode was previously ultrasonically cleaned in aqueous 1.0 or 5.0 mM HAuCl₄ solution for 5 min to remove surface contaminants and drive the air out of the nanotube. Au nanoparticles were then deposited on the TiNT arrays using a potential pulse between a pulse-on and a pulse-off at room temperature. Note that *t*_{on} and *t*_{off} was fixed at 50 and 100 ms, respectively. The potential of pulse-on was varied at -1.0, -2.0, -3.0 and -5.0 V, while the potential of pulse-off was constant at 0 V for 125 cycles of deposition time (one cycle consists of a pulse-on and a pulse-off). The deposition time or pulse cycle was varied at 25, 75, and 125 cycles at condition of 1.0 mM HAuCl₄ and -5.0 V pulse-on. In the pulse electrodeposition process, the current was measured simultaneously by the Autolab potentiostat.

Characterization

Morphologies and structures were examined by field emission scanning electron microscopy (FESEM) and energy-dispersive X-ray spectroscopy (EDS, JSM-7610F). The crystal structure was analyzed with an X-ray diffractometer (XRD, Bruker AXS). Cyclic voltammetry was performed using μAutolab FRAIII with three electrodes. The AuNP-TiNT array acted as the working electrode, while a platinum coil and an Ag/AgCl electrode acted as the counter and reference electrodes, respectively. Cyclic voltammetric experiment for Au nanoparticle characterization was carried out in 1.0 M of NaOH with a potential sweep rate of 100 mV/s.

H₂O₂ detection

The electrochemical measurement for H₂O₂ sensing was performed using μ Autolab FRAIII. The AuNP-TiNT array (or the TiNT arrays) acted as the working electrode (8.0 mm in electrode diameter). A platinum coil and an Ag/AgCl electrode were used as counter and reference electrodes, respectively. Cyclic voltammetric experiment for H₂O₂ sensing was carried out in a 10 mM phosphate buffer saline (PBS, containing 0.1 M KCl, pH 6.0) with a potential sweep rate of 100 mV/s.

Results and Discussion

Figure 1(A) shows the typical anodization current for the growth of TiNT arrays. The current density steeply decreases to 6.11 mA/cm² for the initial stage at 0–40 s because of oxide formation on the Ti surface. The oxide film on the Ti surface impedes the flow of current. After that, the current density slowly decreases because of pore nucleation, reaching a minimum value of current density. Finally, as the anodization proceeds, the nanotube vertical growth is revealed by the progressive current density decay during the remaining anodization time, characteristic of Ti nonsteady state anodization with faster oxidation than dissolution at the nanotube bottom. The resulting TiNT arrays are shown in the FESEM images of Figs. 1(C) and 1(D). From the top view (Fig. 1(C)) and cross-sectional view (Fig. 1(D)), it shows that the TiNT arrays are vertically oriented with a diameter of approximately 150 nm and a wall thickness of about 15 nm. Figure 1(B) shows the distribution of TiNT diameter on the surface. The layer thickness (measured from the cross-sectional view of the FESEM image) is approximately 750 nm.

The as-formed TiNT is amorphous, and to gain a better electronic property, the amorphous TiNT is converted to the anatase phase by annealing at 500°C for 90 min. The typical XRD patterns of Ti, TiNT array, and annealed TiNT array are shown in Fig. 2. The XRD pattern of the pure Ti sample shows the Ti metal phase (JCPDS No. 01-1198). With the as-formed TiNT arrays, only Ti peaks can be observed. This indicates that the nanotubes are amorphous. After annealing, the anatase peak is revealed in Fig. 2 (TiNT 500). This suggests that the TiNT arrays will form to the anatase phase on the Ti surface. Due to the small value of anatase peak, this may yield the small amount of the anatase phase in the TiNT structure. The annealed TiNT arrays were further used for loading Au nanoparticles on their

surfaces by the pulse electrodeposition process.

Figure 3(A) shows an example of alternating pulses in the electrodeposition process for loading the Au nanoparticles on the TiNT array surface using the potentiostat. One cycle in this process consists of a pulse-on and a pulse-off ($t_{\text{on}} = 50$ ms and $t_{\text{off}} = 100$ ms) period. For the pulse-on period, the potential was applied at -3.0 V to the electrode for 50 ms, while for the pulse-off period, the zero potential (0 V) was applied for 100 ms. A longer t_{off} or relaxation period allows time for the metal ion to replenish near the surface. It will enhance the nucleation rate and depressing dendritic growth.²⁵ Figure 3(B) shows an example of a measured current during the pulse electrodeposition. In this experiment, the potential was applied at -5.0 V of pulse-on ($t_{\text{on}} = 50$ ms) and 0 V of pulse-off ($t_{\text{off}} = 100$ ms). The concentration of HAuCl₄ was 1.0 mM. Initially, the current was approximately -0.005 and 0 A for applied pulse-on and pulse-off, respectively. After that, the current slightly increased to approximately 0.001 A for pulse-off and approximately -0.006 for pulse-on (see at 25 cycles). The inset of Fig. 3(B) shows one and three cycles (pulse-on and pulse-off) for the measurement of current in the electrodeposition process. It can be seen that when the pulse-on was applied, the measured current was slightly increased. When switching to pulse-off,

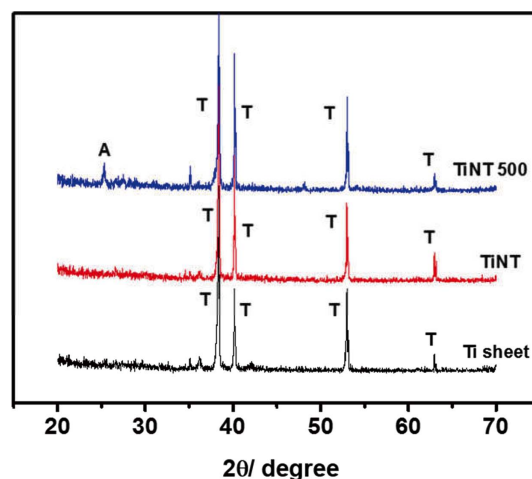


Fig. 2 XRD pattern of the Ti sheet, TiNT array, and annealed TiNT array at 500°C for 90 min (A = anatase, T = titanium).

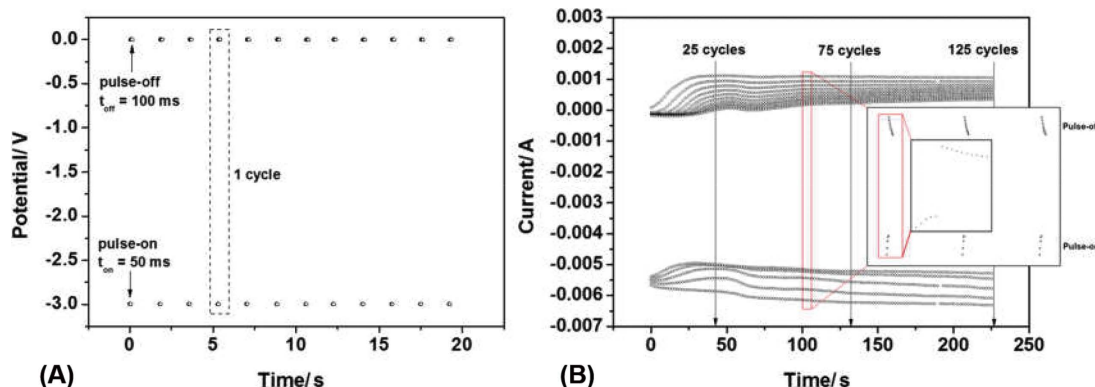


Fig. 3 (A) A series of pulsed electrodeposition for depositing Au nanoparticles and (B) the current was measured during pulse electrodeposition of TiNT arrays in 1 mM HAuCl₄ at -5.0 V of pulse-on and 0 V of pulse-off.

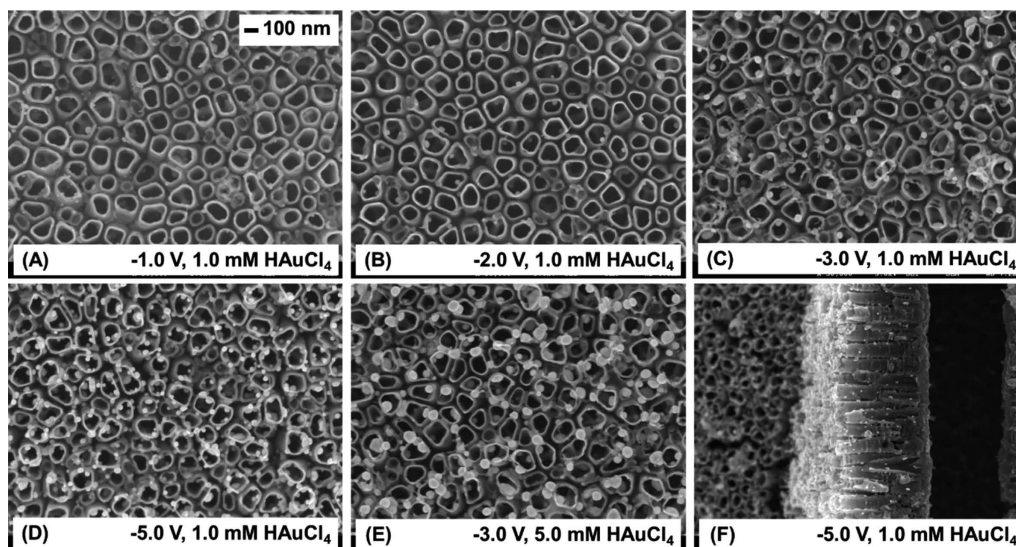


Fig. 4 FESEM image of AuNP-TiNT array prepared by pulse electrodeposition ($t_{\text{on}} = 50$ ms and $t_{\text{off}} = 100$ ms) at a 125-cycle deposition time with various deposition potentials in 1.0 mM HAuCl_4 electrolyte: (A) -1.0 V, (B) -2.0 V, (C) -3.0 V, (D) -5.0 V, (E) -3.0 V at 5.0 mM HAuCl_4 , and (F) cross section of the Au-TiNT array at -5.0 V of applied potential with 1.0 mM HAuCl_4 .

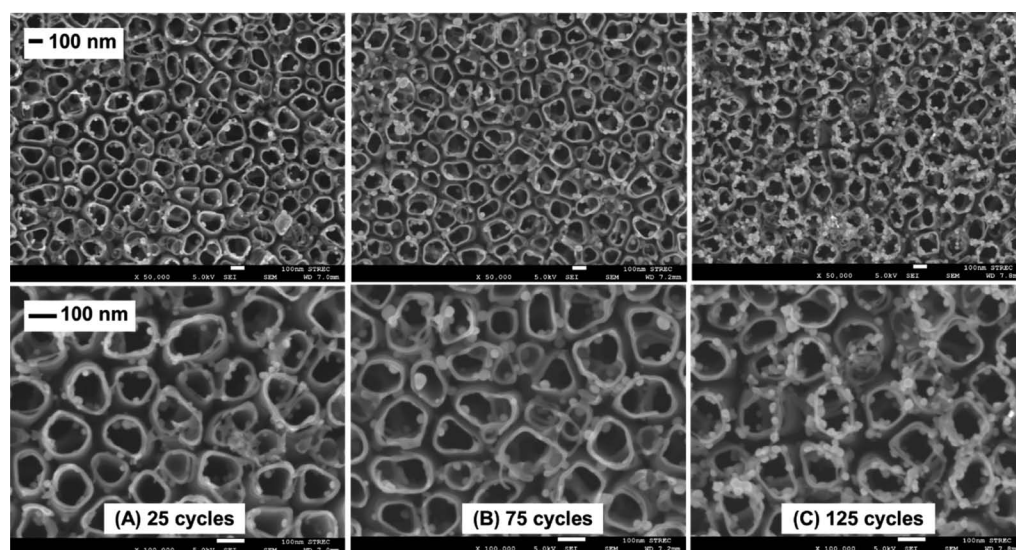


Fig. 5 FESEM image of the AuNP-TiNT array prepared by pulse deposition at applied voltage -5.0 V, $t_{\text{on}} = 50$ ms, and $t_{\text{off}} = 100$ ms with various deposition times: (A) 25, (B) 75, and (C) 125 cycles.

the current was slightly decreased.

Figure 4 shows the FESEM image of Au nanoparticles loading on TiNT arrays; we denote these as AuNP-TiNT arrays. The TiNT array electrode was applied with different potentials compared to the Ag/AgCl electrode in the pulse electrodeposition process. In the reaction, the concentration of the $[\text{AuCl}_4]^-$ solution is lower at the TiNT surface compared to the one far from the surface. The $[\text{AuCl}_4]^-$ solution can be ionized as seen in Eq. (1). The deposition of Au nanoparticles on the TiNT surface can be predicted as in Eq. (2).²⁶



In the pulse-on period, the Au^{3+} is reduced to Au as seen in Eq. (2). This will induce the $[\text{AuCl}_4]^-$ from the bulk solution diffusing onto the TiNT surface. During the pulse-off period, the concentration of $[\text{AuCl}_4]^-$ is replenished at the interface of the electrode. This will decrease the concentration polarization. Consequently, the reduction reaction in Eq. (2) can occur under a high current density to promote the formation of the Au seed on the TiNT surface with grain refinement.

Figures 4(A) – 4(E) and 4(F) show the typical top-view and cross-section-view FESEM images of AuNP-TiNT arrays at different applied potentials for a 125-cycle deposition time with $t_{\text{on}} = 50$ ms and $t_{\text{off}} = 100$ ms. The TiNT arrays display a highly ordered structure and a vertical orientation. As seen in the figure, the Au nanoparticles were spherical and were highly dispersed both outside and inside the TiNT surface, especially

on top of the tube. The amount of Au nanoparticles loading on the TiNT array surface increased with increasing applied potential. The Au nanoparticles seem smaller and the density of Au nanoparticles increases when a high potential was applied (see Fig. 4(D)). This can explain that a high potential is deemed to increase the nucleation rate by increasing free energy.²⁴ Moreover, the size and amount of Au nanoparticles increase with increasing HAuCl₄ concentration (comparing Figs. 4(C) and 4(E)).

Figure 5 shows the effect of deposition time for loading Au nanoparticles on the TiNT array surface. The amount of Au nanoparticles clearly increases with increasing deposition time. Moreover, the size of loaded Au nanoparticles was 10 to 40 nm by varying the pulse cycle from 25 to 125. These results confirmed that the further nucleation and growth of Au nanoparticles are likely to reduce their surface energy.²⁶ Thus, both the size and the loaded amount of Au nanoparticles in the pulse electrodeposition can be adjusted by varying the electrolyte concentration, on-off time, deposition potential, and deposition time.

Figure S1 (Supporting Information) shows the FESEM image, mapping, and EDS spectra of AuNP-TiNT arrays. The surface was prepared in 1.0 mM of HAuCl₄ at -5.0/0 V of potential pulses for 125 cycles. Regarding the EDS spectra, the AuNP-TiNT surface shows the peak of O, Ti, and Au with 35.61, 53.24, and 11.14 %weight, respectively. The AuNP-TiNT arrays are clearly composed of the elements Ti, O, and Au on the surface. The Au element is highly dispersed on the TiNT array surface as seen in the red dot on the map with 11.14 %weight. The ratio between Ti and O corresponds to TiO₂. This result confirms that the Au nanoparticles are dispersed on the TiNT array surface.

Figure 6 shows the cyclic voltammogram of the TiNT array and AuNP-TiNT array in the 1.0 M NaOH solution for determining the Au nanoparticles on the TiNT arrays surface. The AuNP-TiNT reveals the reduction peak at +0.15 V because of the presence of Au nanoparticles on the surface. For the TiNT array sample, there is no reduction peak. This indicates that the TiNT array surface was loaded by Au nanoparticles.

Figure 7 shows the study of electrocatalytic activity toward the reduction of H₂O₂ for comparing the TiNT and AuNP-TiNT electrodes. In Fig. 7(A), it is evident that the AuNP-TiNT-based electrode exhibits a higher electroreduction current in the

presence of H₂O₂ than the bare TiNT electrode. Moreover, the electrochemical reduction of H₂O₂ on the TiNT electrode starts at -0.21 V, while this reaction occurs at -0.022 V on the AuNP-TiNT electrode. The results clearly demonstrate that the reduction of H₂O₂ requires a lower overpotential on the AuNP-TiNT electrode. The enhanced electrocatalytic currents and the positive shifts of the onset potential for the reduction of H₂O₂ can be attributed to the good electroconductivity of Au nanoparticles. Moreover, the uniform dispersed Au nanoparticle on the surface may contribute to the good electroconductivity. Figure 7(B) shows the calibration curves for H₂O₂ on the TiNT and the AuNP-TiNT electrodes. The condition for prepared AuNT-TiNT is 1.0 mM HAuCl₄ and -5.0 V of applied voltage for 125 cycles. Both electrodes exhibit a linear range of 0.5 to 5.0 mM for the detection of H₂O₂. The AuNP-TiNT electrode shows a higher slope than that of the TiNT. This result suggests that the AuNP-TiNT electrodes had higher sensitivity than the TiNT electrode for H₂O₂ sensing. This was due to the presence of AuNPs in the AuNP-TiNT electrode. The limit of detection and sensitivity will be further investigated for H₂O₂ sensing.

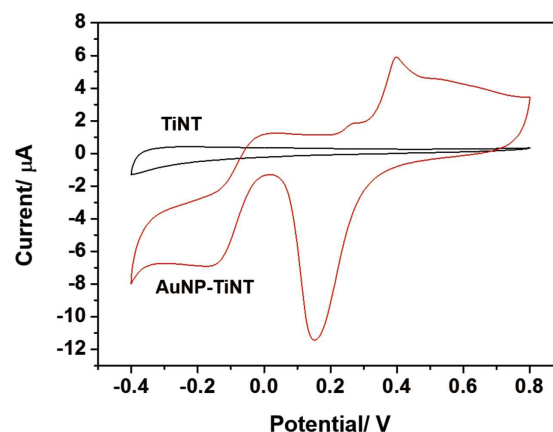


Fig. 6 Cyclic voltammogram of the TiNT array and AuNP-TiNT array in 1.0 M NaOH of electrolyte scanning from -0.4 to 0.8 V with a 100 mV/s scan rate. The AuNP-TiNT array was prepared in 1.0 mM of HAuCl₄ solution at -5.0 V of pulse-on and 0 V of pulse-off for 125 cycles.

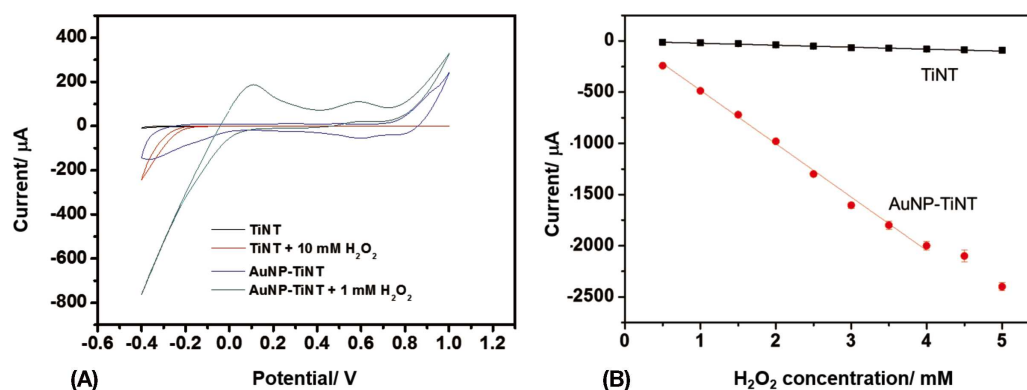


Fig. 7 Cyclic voltammogram of the TiNT and the AuNP-TiNT-based electrodes in a PBS solution with and without H₂O₂ (A). (B) Comparison of calibration curves of response current for H₂O₂ sensing between TiNT and AuNP-TiNT electrodes (condition: -5.0 V of pulse on and 0 V of pulse-off, 1.0 mM HAuCl₄, 125 cycles). The change of current was measured during CV at fixed -0.4 V of applied potential.

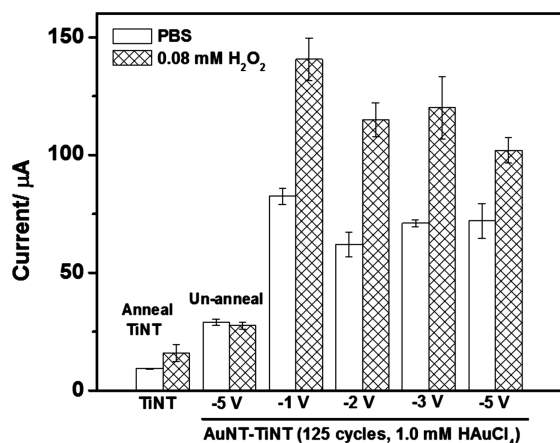


Fig. 8 Comparison of response current for H₂O₂ sensing on the different TiNT electrodes. The current was measured at -0.4 V of applied voltage.

Figure 8 shows the response current for H₂O₂ sensing on the different TiNT array electrodes. The current was measured at -0.4 V of applied voltage in the PBS solution with or without H₂O₂ (0.08 mM of concentration). For the annealed TiNT array electrode, the response current slightly increased after injection of H₂O₂. After modification with Au nanoparticles on the TiNT array electrode, the response current significantly increased for the H₂O₂ sensing comparing to the TiNT array electrode. But for the un-annealed TiNT array electrode, the response current did not change after injection of H₂O₂ for un-annealed TiNT array. This may be because the anatase structure of the TiNT surface will support the sensing of H₂O₂. For the annealed electrode with decorated Au nanoparticles, the response current of those electrodes was not significantly different. The maximum response current was observed for the AuNT-TiNT electrode prepared at -1.0 V of applied potential pulse. It seems that the response currents slightly decrease when increasing the pulse potential (or increasing Au nanoparticles in size and density, see Fig. 4). However, this result shows that the AuNP-TiNT electrodes had higher response current than the TiNT electrode for H₂O₂ sensing. This was due to the presence of Au nanoparticles on the AuNP-TiNT surface.

Conclusions

In this work, we reported the Au nanoparticles that form on tube walls of the self-organized TiNT array using a pulse electrode deposition. The size and density of Au nanoparticles can be controlled by varying the potential and time deposition. We also demonstrated a sensitive H₂O₂-sensing platform, which used the AuNP-TiNT as working electrode. Because of the synergistic effect of Au nanoparticles, the AuNP-TiNT electrode exhibits a higher electrocatalytic activity toward H₂O₂ reduction than the bare TiNT electrode. Moreover, we illustrated that the AuNP-TiNT-based electrode is significant for applications such as electrode substrate for H₂O₂ sensing (compared to conventional electrode materials such as glassy carbon or Au electrodes) and is a feasible platform for the construction of enzyme base biosensors.

Acknowledgements

This work was supported by Srinakharinwirot University (Grant No. 009/2559).

References

1. C. A. Grimes and G. K. Mor, "TiO₂ Nanotube Arrays: Synthesis, Properties, and Applications", **2009**, Springer Science & Business Media, New York.
2. P. M. Perillo and D. F. Rodriguez, *Sens. Actuators, B*, **2012**, 171-172, 639.
3. T. Stoll, G. Zafeiropoulos, and M. N. Tsampas, *Int. J. Hydrogen Energy*, **2016**, 41, 17807.
4. M. K. Arfanis, P. Adamou, N. G. Moustakas, T. M. Triantis, A. G. Kontos, and P. Falaras, *Chem. Eng. J.*, **2017**, 310, 525.
5. C. Wang, Y. Bai, Y. Bai, J. Gao, and W. Ma, *Surf. Coat. Technol.*, **2016**, 286, 327.
6. P. Benvenuto and A. K. M. Kafi, *J. Electroanal. Chem.*, **2009**, 627, 76.
7. W. Wang, Y. Xie, Y. Wang, H. Du, C. Xia, and F. Tian, *Microchim. Acta*, **2014**, 181, 381.
8. A. K. M. Kafi, G. Wu, and A. Chen, *Biosens. Bioelectron.*, **2008**, 24, 566.
9. L. Zhang, D. B. Tian, and J. J. Zhu, *Bioelectrochemistry*, **2008**, 74, 157.
10. Q. Zhao, S. Tang, C. Fang, and Y. F. Tu, *Anal. Chim. Acta*, **2016**, 936, 83.
11. Y. Xie and Y. Zhao, *Mater. Sci. Eng. C*, **2013**, 33, 5028.
12. A. Corma, P. Serna, and H. Garcia, *J. Am. Chem. Soc.*, **2007**, 129, 6358.
13. I. Paramasivalm, J. M. Macak, and P. Schmuki, *Electrochem. Commun.*, **2008**, 10, 71.
14. D. F. Zhang, *Russ. J. Phys. Chem. A*, **2012**, 86, 498.
15. M. Maicu, M. C. Hidalgo, G. Colón, and J. A. Navío, *J. Photochem. Photobiol. A*, **2011**, 217, 275.
16. L. Sun, J. Li, C. Wang, S. Li, Y. Lai, H. Chen, and C. Lin, *J. Hazard. Mater.*, **2009**, 171, 1045.
17. A. Karci, I. Arslan-Alaton, and M. Bekbolet, *J. Hazard. Mater.*, **2012**, 263, 275.
18. Q. Wang, X. Yang, D. Liu, and J. Zhao, *J. Alloys Compd.*, **2012**, 527 106.
19. C. Wang, Y. Bai, Y. Bai, J. Gao, and W. Ma, *Surf. Coat. Technol.*, **2016**, 286, 327.
20. L. Hu, C. C. Fong, X. Zhang, L. L. Chan, P. K. S. Lam, P. K. Chu, K. Y. Wong, and M. Yang, *Environ. Sci. Technol.*, **2016**, 50, 4430.
21. Y. Lai, H. Zhuang, K. Xie, D. Gong, Y. Tang, L. Sun, C. Lin, and Z. Chen, *New J. Chem.*, **2010**, 34, 1335.
22. L. Wu, F. Li, Y. Xu, J. W. Zhang, D. Zhang, G. Li, and H. Li, *Appl. Catal. B*, **2015**, 164, 217.
23. X. Li, J. Yao, F. Liu, H. He, M. Zhou, N. Mao, P. Xiao, and Y. Zhang, *Sens. Actuators, B*, **2013**, 181, 501.
24. M. S. Chandrasekar, Shanmugasigamani, and M. Pushpavanam, *Mater. Chem. Phys.*, **2009**, 115, 603.
25. L. Assaud, V. Heresanu, M. Hanbucken, and L. Santinacci, *C. R. Chim.*, **2013**, 16, 89.
26. L. X. Yang, S. L. Luo, F. Su, Y. Xiao, Y. F. Chen, and Q. Y. Cai, *J. Phys. Chem. C*, **2010**, 114, 7694.